

# Hybrid Organic/Inorganic Molecular Heterojunctions Based on Strained Nanomembranes

Carlos Cesar Bof Bufon,<sup>\*,†</sup> Juan Diego Arias Espinoza,<sup>†</sup> Dominic J. Thurmer,<sup>†</sup> Martin Bauer,<sup>†</sup> Christoph Deneke,<sup>†,||</sup> Ute Zschieschang,<sup>§</sup> Hagen Klauk,<sup>§</sup> and Oliver G. Schmidt<sup>†,‡</sup>

<sup>†</sup>Institute for Integrative Nanosciences, IFW-Dresden, Helmholtz Strasse 20, 01069 Dresden, Germany

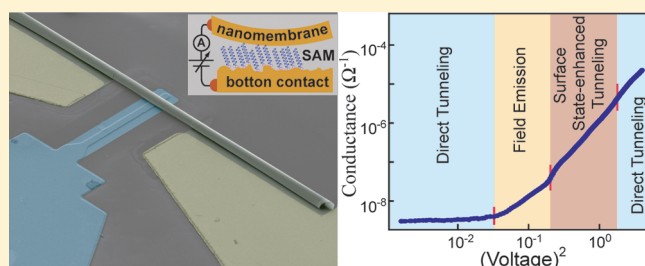
<sup>‡</sup>Material Systems for Nanoelectronics, TU-Chemnitz, Reichenhainer Strasse 70, 09107 Chemnitz, Germany

<sup>§</sup>Max Planck Institute for Solid State Research, Heisenberg Strasse 1, 70569 Stuttgart, Germany

**S** Supporting Information

**ABSTRACT:** In this work, we combine self-assembly and top-down methods to create hybrid junctions consisting of single organic molecular monolayers sandwiched between metal and/or single-crystalline semiconductor nanomembrane based electrodes. The fabrication process is fully integrative and produces a yield loss of less than 5% on-chip. The nanomembrane-based electrodes guarantee a soft yet robust contact to the molecules where the presence of pinholes and other defects becomes almost irrelevant. We also pioneer the fabrication and characterization of semiconductor/molecule/semiconductor tunneling heterojunctions which exhibit a double transition from direct tunneling to field emission and back to direct tunneling, a phenomenon which has not been reported previously.

**KEYWORDS:** Electronic materials and devices, molecular self-assembly, nanoscale materials, organic–inorganic nanostructures, nanomembranes, strain engineering



The creation of organic/inorganic hybrid heterojunctions opens the possibility for new functional elements previously not feasible by either component individually. Simple metal/molecule junctions have already proven highly useful for a variety of applications.<sup>1</sup> By adding the robustness and high carrier mobility of an inorganic semiconductor in combination with the tailorability and processability of organic materials, novel electronic elements such as hybrid resonant-tunneling diodes and field-effect transistors<sup>2</sup> can be realized. It is not always possible to combine materials of different nature in a favorable way, however. Most common deposition methods for metallic electrodes often have devastating effects on ultrathin molecular layers,<sup>3</sup> for instance. Similarly, the creation of heterojunctions consisting of well-defined periods of epitaxial semiconductors (such as GaAs, Si, or SiGe), which typically require high growth temperatures (200–1000 °C), and single organic monolayers cannot be fabricated by standard layer-by-layer deposition techniques.<sup>4,5</sup>

Incorporating semiconductor contacts and molecular monolayers provides an exciting alternative to further expand the horizons of molecular electronics. First, such electrodes create an additional degree of freedom for manipulating the charge flow in the organic layers.<sup>6,7</sup> Furthermore, a high level of control can be achieved by tuning the position of the Fermi level within the semiconductor band gap via the precise adjustment of dopant material and density.<sup>8</sup> Second, the reproducibility and stability of molecular junctions are strongly correlated with the flatness of

the electrode.<sup>9</sup> The use of single-crystalline semiconductors, which have surfaces intrinsically smoother than metallic layers (such as Au and Ag), is of a great advantage in this respect. While several other methods have previously been demonstrated for creating single self-assembled molecular layers (SML), which are then sandwiched between metal and semiconductor contacts,<sup>7,10–12</sup> the fabrication and electrical characterization of semiconductor/SML/semiconductor heterojunctions using epitaxially grown materials is still lacking.

Self-assembly methods have been widely employed not only for depositing organic monolayers<sup>13</sup> but also for the formation of micro- and nano-objects.<sup>14–16</sup> A typical example of such an approach is the creation of three-dimensional electronic elements based on self-wound nanomembranes which can be manufactured in parallel on-chip.<sup>17–19</sup>

Here, we present a method for preparing hybrid organic/inorganic heterojunctions using strained metal and/or semiconductor nanomembranes as electrodes. In this way, heterojunctions consisting of metal/SML/metal, semiconductor/SML/semiconductor and combinations thereof are created. In the latter cases, the semiconductor doping type and concentration can be independently adjusted for each electrode in order to tune the

**Received:** May 25, 2011

**Revised:** August 4, 2011

**Published:** August 09, 2011

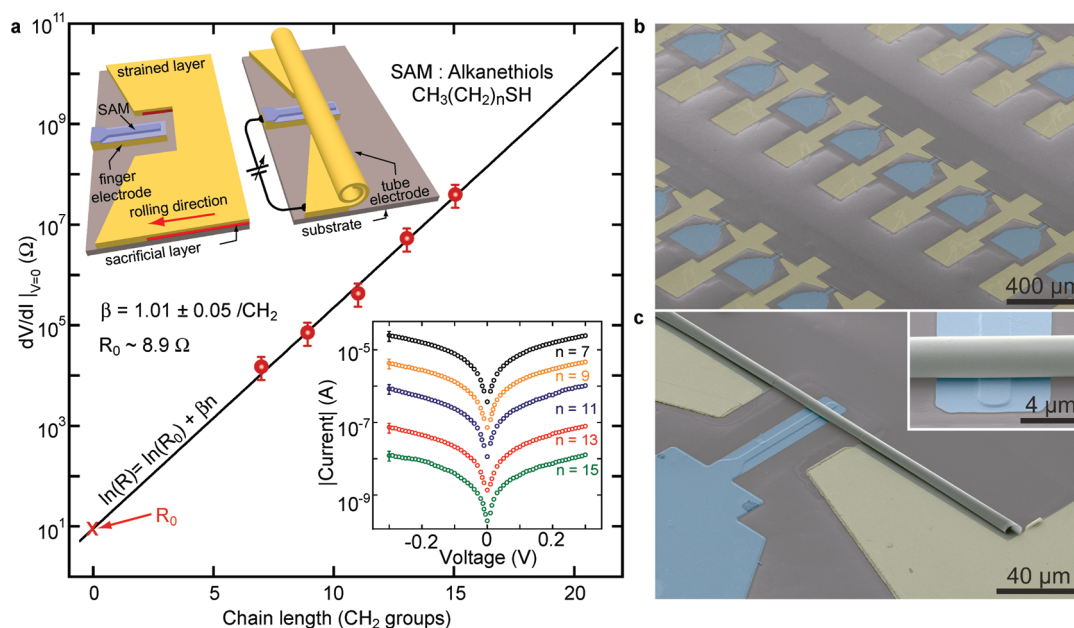


**Figure 1.** (a) Differential resistance at zero bias condition ( $R = dV/dI|_{V=0}$ ) as a function of the number of  $\text{CH}_2$  groups (obtained from the  $i-v$  characteristics displayed in the bottom inset) for Au-alkanethiol SAM/Au heterojunctions. Chemisorption and physisorption are indicated by “-” and “/”, respectively. By using eq 1,  $\beta$  was found to be  $1.01 \pm 0.05/\text{CH}_2$  and  $R_0 \sim 8.9 \Omega$ . The upper insets show (left) the device structure before rolling and (right) after rolling. The strained layer consists of a trimetallic nanomembrane patterned on top of a sacrificial layer (details in the Supporting Information). Once the sacrificial layer is selectively removed, the strained layer curls toward the Au finger structure (with a roughness of  $\sim 0.36 \text{ nm rms}$ ). After the rolling process the tube-shaped electrode rests on top of the Au finger establishing an electrical connection through the alkanethiol SAM, with chain lengths ranging from 7 to 15  $\text{CH}_2$  groups, which were previously grown on the finger surface. (b) Scanning electron microscope (SEM) image of an array of devices highlighting the excellent reproducibility and parallelism of the fabrication process with a yield of at least 95%. (c) SEM image of a single element. The inset highlights the overlap of the tube and metallic finger electrode.

device’s electronic properties. By incorporating the self-rolling phenomenon,<sup>14–16</sup> we have developed an approach which is fully integrative on-chip, using well-established semiconductor processing technologies. In this way, several components can be fabricated in parallel with high yield (>95%) while the active contact area remains well below  $1 \mu\text{m}^2$ . The strained nanomembrane-based electrodes provide a soft yet robust contact on top of the SML, where damages to the molecules are minimized and short circuits via pinholes are absent. Furthermore, we present the fabrication and characterization of hybrid heterojunctions having n- and p-doped crystalline semiconducting nanomembranes as electrodes, contacting self-assembled monolayers (SAM). These heterojunctions exhibit electronic properties including the sequential double transition from direct tunneling to field emission and back to direct tunneling which has not been observed for either element separately.

The “simplest” hybrid molecular structure proposed to date is the metal/SML/metal junction. The main challenge for fabricating such structures lies in the ability of placing the metal electrode in intimate contact with the molecular layer without damaging its intrinsic properties or affecting the overall junction stability and reproducibility.<sup>20</sup> The situation becomes more complex when single molecular layers, prepared by self-assembly for instance, are required. Here, the inevitable presence of pinholes and defects<sup>21</sup> over a long-range has been addressed by different contacting approaches,<sup>3</sup> to enable the use of such monolayers for device applications.<sup>22,23,25</sup>

The upper inset in Figure 1a shows a sketch of a device concept to prepare metal/SML/metal heterojunctions based on rolled-up metallic nanomembranes. A detailed description of the

device fabrication is included in the Supporting Information. The rolling is caused by the self-release of a strained metallic nanomembrane by selectively etching away the underlying sacrificial layer. After the rolling process, a tube-shaped electrode rests on top of the metallic finger, establishing an electrical connection through the alkanethiol SAM (Figure 1c).

For these experiments gold (Au) layers are incorporated into the strained metallic nanomembrane producing Au-alkanethiol SAM/Au junctions after rolling, as indicated in the figure. Due to the nature of this fabrication approach, the devices can be patterned in parallel on-chip and can even be integrated with pre-existing structures on a wafer. Figure 1b shows an SEM image of an array of devices highlighting the excellent reproducibility of the fabrication process. The image was taken from a sample with a yield loss of less than 5%.

To characterize the electronic properties of the Au-alkanethiol SAM/Au junctions, a positive bias is applied to a finger electrode to which the molecules are chemically bonded (inset of Figure 1a). For statistical purposes, current–voltage ( $i-v$ ) traces were obtained for at least 10 devices of each alkanethiol chain length (inset graph of Figure 1a). Similar to previously reported work using other contacting methods,<sup>24–27</sup> the  $i-v$  characteristics indicate that the current is strongly dependent on the SAM chain length. Since the experiments are performed under low bias, no significant asymmetry that might otherwise have been caused by the different contact configurations (i.e., tube/ $\text{CH}_3$  physisorbed and finger-S chemisorbed) was observed.<sup>28</sup> In Figure 1, the systematic change of the chain length furthermore reveals direct tunneling (DT) as the dominant transport mechanism.<sup>24,25</sup> As expected for coherent and nonresonant

tunneling, the differential resistance ( $R = dV/dI|_{V=0}$ ) exhibits an exponential dependence on the chain length as given by<sup>25,29</sup>

$$R = R_0 \exp(\beta n) \quad (1)$$

where  $R_0$  is the total contact resistance (see Supporting Information),  $n$  is the tunneling barrier thickness (here, the number of  $\text{CH}_2$  groups in the alkyl chain), and  $\beta$  is the exponential decay factor which has been reported<sup>25,30</sup> as ranging from 1.0 to 1.8 per  $\text{CH}_2$  group. By using eq 1,  $\beta$  was found to be  $1.01 \pm 0.05/\text{CH}_2$ , which is in accordance with the accepted values for  $\sigma$ -saturated molecules.<sup>25,31,32</sup> Through comparison with other charge transport measurements in identical molecular systems,<sup>24,33</sup> we have estimated a junction contact of roughly  $0.27 \mu\text{m}^2$  in our system. If we assume a full molecular coverage of the finger surface ( $S$  molecules/ $\text{nm}^2$ ),<sup>33</sup> the transport across the rolled-up junction is probing roughly  $10^6$  molecules. Naturally, the existence of pinholes and other defects can also be present at the junction interface.<sup>21</sup> However, the tube electrode softly resting on top of the SAM selectively contacts the highest chains and ignores the presence of pinholes and defective (possibly tilted) chains which are shorter than the ones standing more upright. Although rolled-up nanomembranes can be used to prepare soft, reproducible, and wrinkle-free contacts for molecular layers, the geometric contact area of such junctions cannot be directly quantified by optical methods presently, and thus we rather rely on the uniformity given by the electrical measurements.

In addition to contacting molecules with metallic electrodes, we also demonstrate an approach where semiconductor layers are used to inject charge into and through the molecular layers. Figure 2a is a sketch of the layer structure before the release of the semiconducting nanomembrane, while Figure 2b highlights the exact layer composition (details in Supporting Information).

The unrolled device creates a p–i–n structure having a p-type GaAs layer (p:GaAs) as the top electrode. Alternatively, an Au thin film can replace the p:GaAs to form a planar metal–insulator–semiconductor (MIS) diode. Before the semiconductor layer is rolled up, a SAM of hexadecylphosphonic acid (C16PA) is chemically adsorbed<sup>6,8</sup> onto the p:GaAs layer (labeled here as p:GaAs–C16PA). In contrast, a hexadecanethiol monolayer (C16S) is self-assembled when using an Au covering layer. By selectively removing the AlAs sacrificial layer in a 3.1 vol % HF:DI– $\text{H}_2\text{O}$  solution, the strained semiconductor nanomembrane curls in such a way that the bottom n-doped  $\text{In}_{20}\text{Ga}_{80}\text{As}$  (n:InGaAs) layer mechanically contacts the top of the heterostructure establishing an electrical connection (Figure 2c). In addition to the p:GaAs–C16PA/n:InGaAs, a p:GaAs/n:InGaAs p–n heterojunction can be formed by rolling if one merely omits the SAM deposition step. Alternatively, when the Au film is used, a mechanically assembled metal/semiconductor heterojunction (Au/n:InGaAs) can be realized. Importantly, the incorporation of a SAM leads to new types of p–i–n and MIS structures, where the insulating barrier is now the organic SAM.

In the rolled-up architecture (Figure 2c), a voltage bias applied between the top and back contacts creates a current that can flow into the top p:GaAs electrode. Subsequently it is radially injected across the C16PA layer and then into the n:InGaAs nanomembrane. The current flows tangentially around the n:InGaAs tube wall and is then collected via the back contact. A similar concept is still valid if the p:GaAs layer is replaced by the Au film.

In the unrolled device, the measured current ( $I_M$ ) originates solely from the leakage through the AlGaAs barrier ( $I_b$ ). In the

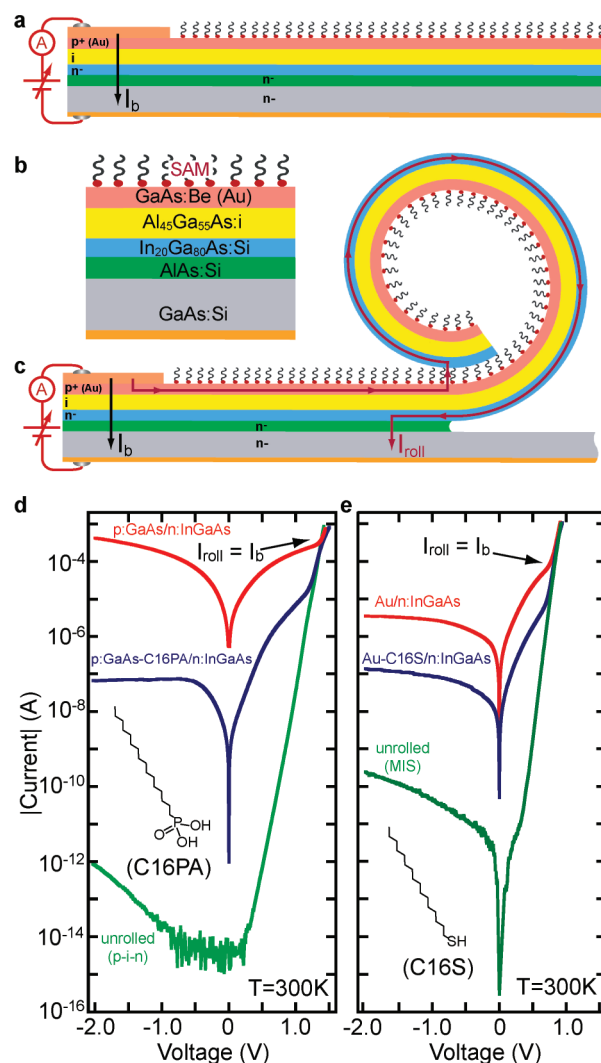


**Figure 2.** (a) Schematic of a multilayer semiconductor device before rolling (details in Supporting Information). The detailed layer structure for the unrolled devices, including the SAM, is revealed in (b). The rolled-up device (c) is formed after the selective removal of the sacrificial layer. The current pathways are highlighted in the figure (a, c). The  $i$ – $v$  characteristics for the heterojunctions having p-doped GaAs as a top layer, before and after rolling, with and without the SAM incorporation are shown in (d). Similarly the traces for heterojunctions incorporating Au as a top layer are shown in (e). The molecular structure of the hexadecylphosphonic acid (C16PA) and hexadecylthiol (C16S) are also shown in the inset of (d) and (e), respectively.

rolled-up device however,  $I_M$  becomes a combination of the tangential current around the n:InGaAs nanomembrane ( $I_{\text{roll}}$ ) and  $I_b$  (Figure 2c). The comparison between rolled and unrolled devices is shown in Figure 2d. At reverse bias  $I_M$  is below 1 pA ( $I_M = I_b$ ) in the unrolled device. At the same bias conditions, an increase of at least 8 orders of magnitude is observed after the formation of the p:GaAs/n:InGaAs heterojunction ( $I_M = I_b + I_{\text{roll}}$ ). This observation is clear evidence of the radial injection and tangential transport across the rolled-up semiconductor nanomembrane. At high forward bias,  $I_b$  increases exponentially and dominates for  $V > 1\text{V}$  ( $I_b > I_{\text{roll}}$ ). Here all  $i$ – $v$  curves merge into a single trace and the maximum allowed forward bias in the

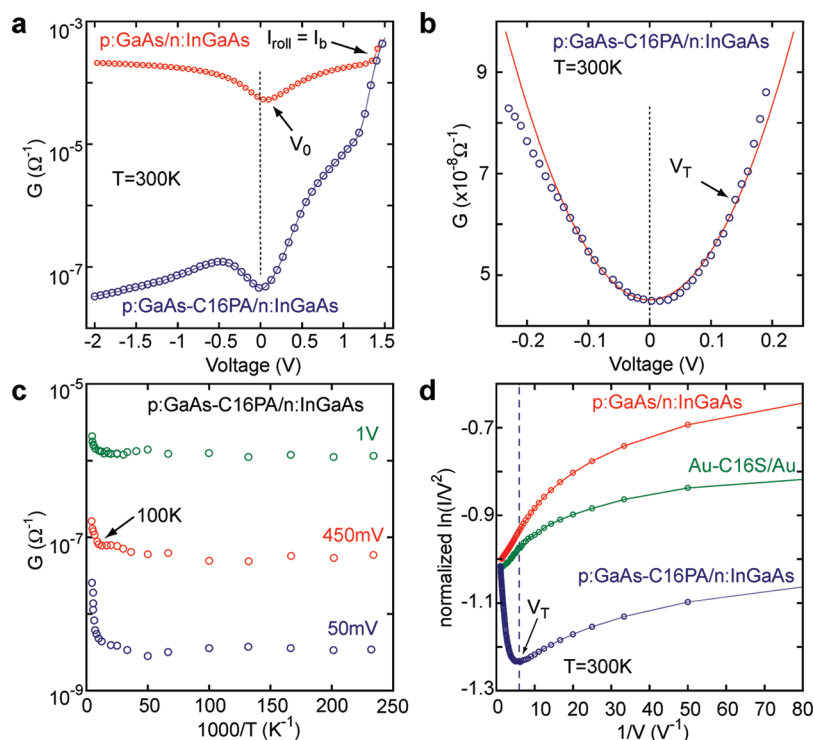


**Figure 3.** Conductance ( $G$ ) of semiconductor nanomembrane-based devices. In (a) the difference between devices with (blue) and without (red) a SAM is shown. A fit to the Simmons model (eq 2) at low bias voltage is shown in (b) for the p:GaAs-C16PA/n:InGaAs heterojunction. The temperature dependence of  $G$  is shown in (c). Between 300 and 100 K hopping across the interfaces contributes to the transport. Below 100 K, tunneling becomes the main transport mechanism. The plot in (d) indicates the transition from direct tunneling (DT) to field emission (FN) at  $V = V_T$ .

rolled-up junction can be defined as the point at which  $l_b = 0.1l_{\text{roll}}$ . As shown in Figure 2e, the behavior of the MIS structure after rolling is qualitatively similar to the  $p-i-n$  device.

The incorporation of the C16PA SAM leads to a drop in the conductance ( $G = I/V$ ) which is furthermore bias dependent (Figure 3a):  $G$  decreases by 4 orders of magnitude at reverse bias while at forward bias a drop of almost 2 orders is observed. While the overall reduction of  $G$  is considered to be an indication that the molecular layer acts as an ultrathin ( $\sim 2$  nm)<sup>34</sup> organic insulator on the nanometer scale,<sup>35,36</sup> the bias dependence can be correlated with the asymmetric nature of the junctions.<sup>36–38</sup> Furthermore, when C16PA is incorporated in the  $p-n$  junction, the minimum value of  $G$  shifts from a voltage  $V_0$  to zero as indicated in Figure 3a. In Figure 3b, the curve agrees very well with the Simmons equation for the conductance<sup>39</sup> at low voltages

$$G \cong G_0(1 + CV^2) \quad (2)$$

where  $G_0$  is the equilibrium conductance and  $C$  is the cubic coefficient related to the barrier shape.<sup>40</sup> Similar to junctions incorporating alkanes (Figure 1), DT across a rectangular-like potential barrier is assumed as the main transport mechanism in the range of  $V \pm 160$  mV.

Despite the fact that a perfect bonding can be formed at several points of the junction after the mechanical contact,<sup>41,42</sup> defects, as well as a thin oxide layer,<sup>43</sup> may be influencing the overall rolled-up junction characteristics by creating interface states. Therefore, in addition to DT, the temperature dependence of  $G$  (Figure 3c) suggests that between 300 and 100 K a small fraction of the transport takes place via hopping through such interface states.<sup>24</sup> Below 100 K,  $G$  clearly becomes temperature-independent indicating that the hopping process is suppressed.

Typically, for metal/insulator/metal junctions, once  $V > \Phi$  (where  $\Phi$  is the barrier height), a change in the barrier shape from rectangular to triangular leads to a transition of the transport mechanism from DT to field emission, also known as Fowler–Nordheim tunneling (FN).<sup>44</sup> In this new regime, the current is described by<sup>45</sup>

$$I \propto V^2 \exp\left(-\frac{4W\sqrt{2m_e}\Phi^3}{3\hbar qV}\right) \quad (3)$$

where  $W$  is the barrier width and  $q$  the electronic charge. The transition from DT to FN has been previously observed in junctions consisting of short<sup>46</sup> aliphatic molecules and  $\pi$ -conjugated molecules.<sup>38</sup> However, to the best of our knowledge, such transition has never been reported for junctions containing longer alkanes (here, C16PA is the tunneling barrier). The main reason is that both the height and width of such molecular barrier are considered relatively large ( $\sim 1.45$  eV and  $\sim 2$  nm, respectively), such that the tunneling probability across the molecular orbital decreases significantly.<sup>8,24,34</sup> Nevertheless, as is shown in Figure 3d by plotting the normalized value of  $\ln(I/V^2)$  as a function of  $1/V$  at room temperature, the p:GaAs-C16PA/n:InGaAs rolled-up heterojunctions display a clear transition around 160 mV. Since this transition occurs at fairly low potentials ( $V_T \sim 160$  mV) compared to the reported<sup>24</sup> values for  $\Phi$  for alkyl chains, we conclude that this effect cannot be directly correlated with a shape transition of the C16PA potential barrier (as observed for the  $\pi$ -conjugated molecules<sup>38</sup>) but rather comes from a combination of the semiconducting and molecular layers. This is seen more clearly in Figure 3d, where, apart from the p:GaAs-C16PA/n:InGaAs heterojunctions, none of the other junctions exhibit the DT-FN type of transition.

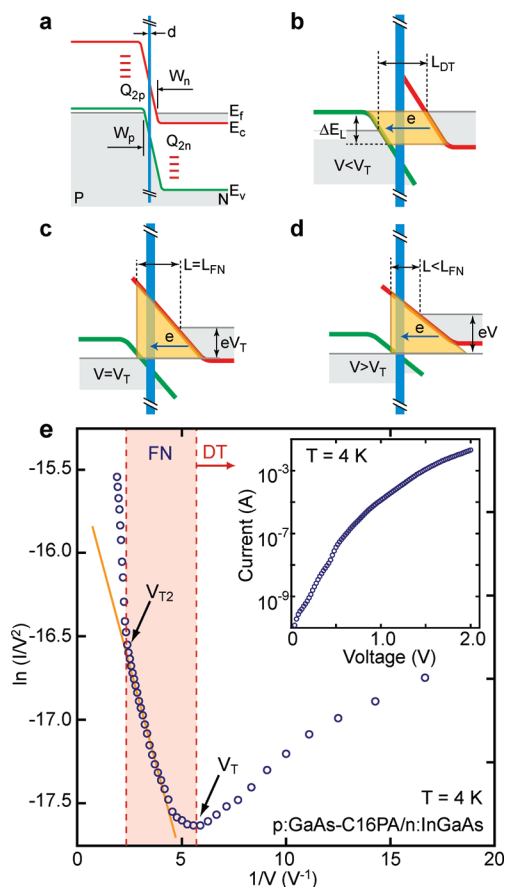


**Figure 4.** (a–d) Band diagram schematics (not to scale) for the p:GaAs-C16PA/n:InGaAs heterojunction under different bias conditions. (a) In equilibrium the Fermi level in the p side of the junction, which is below the top of the valence band (VB), is aligned to the Fermi level at the n side, which sits above the bottom of the conduction band (CB). (b) A zoom of the central region of the band structure shows a rectangular-like barrier that is present at low bias condition ( $V < V_T$ ). As the voltage bias increases, the hybrid barrier shape changes from rectangular (b) to triangular (c) at  $V = V_T$ . At this point a transition from DT to FN is observed (e). For  $V > V_T$ , FN dominates (d) until both  $W_p$  and  $W_n$  become field independent. In (e) the clear transition from DT to FN to DT is shown, indicated by the linear fit for FN tunneling in the intermediate region (the inset highlights the measured  $i-v$  trace).

In Figure 4a a simple band structure model (not to scale) is proposed for such a junction at zero bias condition. The hybrid barrier is assumed to be a combination of the C16PA molecular barrier ( $d$ ) with the potential barriers at the chemisorbed p:GaAs-C16PA ( $W_p$ ) and physisorbed C16PA/n:InGaAs ( $W_n$ ) interfaces of the junction. Due to the high density of charges in the semiconducting layers, the Fermi level on the p-doped interface is below the top of the valence band (VB) while at the n-doped interface it sits above the bottom of the conduction band (CB).<sup>45</sup> By comparing the value of  $\Phi$  reported for alkyl chains bonded to p:GaAs ( $1.1 \pm 0.3$  eV)<sup>8</sup> with the maximum applied voltage used to characterize the junctions, we assume that most changes in the total width/shape of the hybrid tunneling barrier ( $L = W_p + W_n + d$ ) can be attributed to  $W_p$  and  $W_n$ , which are sandwiching the molecular layer. Due to the asymmetric nature of both semiconducting electrodes, the changes of  $W_p$  and  $W_n$  as the voltage bias increases are expected to be different.

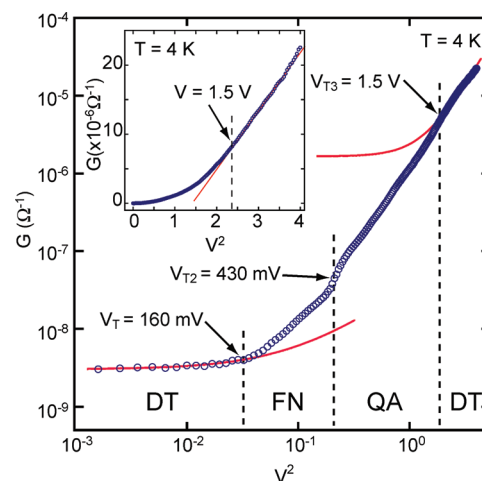


**Figure 5.** All transitions observed for the p:GaAs-C16PA/n:InGaAs heterojunction at 4 K. The fitting lines represent the agreement with the Simmons model (eq 2) and define the region where DT take place. In the intermediate region, both FN and surface-state-enhanced tunneling (QA) takes place. For  $V > 1.5$  V, DT is once again recovered.

As illustrated in Figure 4b, for low forward bias, DT occurs across the rectangular-like potential barrier (with  $L = L_{DT}$ ) since the band bending is not very pronounced and an overlap between the filled levels in the CB and the empty levels in the VB is expected. Once the potential increases (Figure 4c), this overlap decreases and, associated with an asymmetric change of  $W_p$  and  $W_n$ , the tunneling probability becomes strongly voltage-dependent. At the transition voltage  $V_T$ , the hybrid barrier assumes a triangular-like shape (with  $L = L_{FN}$ ) and the transition from DT to FN occurs. For  $V > V_T$ , the transport is mainly field dependent with a systematic decrease of the tunneling distance as the voltage increases (Figure 4d). For  $V \gg V_T$ , we expect that both  $W_p$  and  $W_n$  reach their minimum width and become bias independent.<sup>45</sup> Consequently, DT once more becomes the dominant transport mechanism with tunneling occurring from the CB to VB across the rectangular-like potential barrier. This second transition (FN to DT), however, was not clearly observed at room temperature using the possible voltage range.

To increase the voltage operation range at forward bias, the sample was cooled to 4 K to reduce the thermoactivated transport across the insulating AlGaAs barrier.<sup>45,47</sup> By lowering the temperature, we were able to extend the maximum forward bias to nearly 2 V (see the  $i-v$  curve in the inset of Figure 4e) and, additionally, to reduce the contributions of the surface states to the transport (Figure 3c).<sup>45,47</sup>

Similar to the observations at room temperature, the plot of  $\ln(I/V^2)$  vs  $I/V$  measured at 4 K indicates a clear transition from DT to FN near  $V_T \sim 160$  mV as shown in Figure 4e. This result indicates that  $V_T$  does not change with temperature, supporting the assumption that even with hopping transport taking place at room temperature, tunneling is still the dominant transport mechanism. By further increasing the positive bias, a deviation from the FN mode is observed at  $V_{T2} \sim 430$  mV, while a full recovery of the DT is observed at  $V > 1.5$  V. After the second transition the charge carrier transport occurs with a small influence of  $W_p$  and  $W_n$ . In the voltage range between 430 mV and 1.5 V, the transport most probably is assisted by the interface states (QA) sitting near the semiconductor energy gap midpoint.<sup>47</sup> A more rigorous investigation of this effect is still needed for clarification.

The plot in Figure 5 summarizes all the transitions observed for the p:GaAs-C16PA/n:InGaAs heterojunction. The inset indicates that the agreement with the Simmons model is recaptured at high voltages, highlighted by the linearity above  $\sim 1.5$  V. The agreement with the theoretical calculations (red lines) is clearly seen here also.

In conclusion, we have demonstrated a reliable approach to contact molecular layers with a contact area much smaller than  $1 \mu\text{m}^2$  using conventional semiconductor processing methods. The fabrication process is highly integrative, and several devices can be processed in parallel with a yield higher than 95%. We have shown the assembly and characterization of a hybrid semiconductor/SML/semiconductor heterojunction, where epitaxially grown III–V nanomembranes are used as charge injectors in self-assembled organic monolayers. This system displays unique transport characteristics, namely, the sequential transition from direct tunneling to field emission and then returning to direct tunneling. Consequently, by connecting molecular layers with semiconducting contacts, devices with completely different electronic characteristics are created where such characteristics are not expected, or possible, using either element separately. Furthermore, we have shown that it is possible to use Au as an electrode material in order to create new MIS structures.

In comparison to similar methods for contacting molecular layers, namely, membrane transfer,<sup>11</sup> our approach can be used to create molecular contacts using a wrinkle-free electrode made out of different material classes. In addition, such contacts can be precisely positioned wherever they are needed by deterministic self-assembly of strained nanomembranes.

There is no technical limitation for rolling up other metallic strained layers including Cr, Ti, Co, Fe<sub>3</sub>Si, and Nb<sup>17,19,48,49</sup> to create different junctions specifically incorporating magnetic and/or superconducting materials. Analogous to the III–V materials, similar experiments using epitaxial Si and Ge<sup>18,50</sup> as tubes and fingers could present another variety of hybrid devices. Finally more complex functional molecules<sup>1</sup> can be incorporated, such that the final device behavior combines the electrode's physical characteristics and the molecule's properties.

## ■ ASSOCIATED CONTENT

**S Supporting Information.** Detailed fabrication processes and characterization methods. This material is available free of charge via the Internet at <http://pubs.acs.org>.

## ■ AUTHOR INFORMATION

### Corresponding Author

\*E-mail: [c.bufon@ifw-dresden.de](mailto:c.bufon@ifw-dresden.de).

### Present Addresses

<sup>||</sup>Laboratório Nacional de Nanotecnologia, Caixa Postal 6192, Campinas, S.P., Brazil.

## ■ ACKNOWLEDGMENT

The authors acknowledge D. Grimm, R. Engelhard, F. Cavallo, I. Mönch, and A. Vilan for fruitful discussions and technical support. J. D.A.E. acknowledge MICIT for the partial financial support. The work was financially supported by the DFG FOR 1154 "Towards Molecular Spintronics" and the DFG priority program "Nano-Thermoelektrik".

## ■ REFERENCES

- (1) Heath, J. R.; Ratner, M. A. *Phys. Today* **2003**, *56* (5), 43–49.
- (2) Kagan, C. R.; Mitzi, D. B.; Dimitrakopoulos, C. D. *Science* **1999**, *286* (5441), 945–947.
- (3) Haick, H.; Cahen, D. *Acc. Chem. Res.* **2008**, *41* (3), 359–366.
- (4) Deneke, C.; Zschieschang, U.; Klauk, H.; Schmidt, O. G. *Appl. Phys. Lett.* **2006**, *89* (26), 263110.
- (5) Blumstengel Blumstengel, S.; Sadofev, S.; Puls, J.; Henneberger, F. *Adv. Mater.* **2009**, *21* (47), 4850.
- (6) Shpaisman, H.; Salomon, E.; Neshet, G.; Vilan, A.; Cohen, H.; Kahn, A.; Cahen, D. *J. Phys. Chem. C* **2009**, *113* (8), 3313–3321.
- (7) Vilan, A.; Shanzer, A.; Cahen, D. *Nature* **2000**, *404* (6774), 166–168.
- (8) Neshet, G.; Shpaisman, H.; Cahen, D. *J. Am. Chem. Soc.* **2007**, *129* (4), 734–735.
- (9) Weiss, E. A.; Chiechi, R. C.; Kaufman, G. K.; Kriebel, J. K.; Li, Z. F.; Duati, M.; Rampi, M. A.; Whitesides, G. M. *J. Am. Chem. Soc.* **2007**, *129* (14), 4336–4349.
- (10) Loo, Y. L.; Lang, D. V.; Rogers, J. A.; Hsu, J. W. P. *Nano Lett.* **2003**, *3* (7), 913–917.
- (11) Vilan, A.; Cahen, D. *Adv. Funct. Mater.* **2002**, *12* (11–12), 795–807.
- (12) Lodha, S.; Janes, D. B. *Appl. Phys. Lett.* **2004**, *85* (14), 2809–2811.
- (13) Whitesides, G. M.; Grzybowski, B. *Science* **2002**, *295* (5564), 2418–2421.
- (14) Stoney, G. G. *Proc. R. Soc. London, Ser. A* **1909**, *82* (553), 172–175.
- (15) Schmidt, O. G.; Eberl, K. *Nature* **2001**, *410* (6825), 168–168.
- (16) Prinz, V. Y.; Seleznev, V. A.; Gutakovskiy, A. K.; Chehovskiy, A. V.; Preobrazhenskii, V. V.; Putyato, M. A.; Gavrilo, T. A. *Phys. E (Amsterdam, Neth.)* **2000**, *6* (1–4), 828–831.
- (17) Bufon, C. C. B.; Gonzalez, J. D. C.; Thurmer, D. J.; Grimm, D.; Bauer, M.; Schmidt, O. G. *Nano Lett.* **2010**, *10* (7), 2506–2510.
- (18) Cavallo, F.; Songmuang, R.; Schmidt, O. G. *Appl. Phys. Lett.* **2008**, *93* (14), 143113.
- (19) Thurmer, D. J.; Bufon, C. C. B.; Deneke, C.; Schmidt, O. G. *Nano Lett.* **2010**, *10* (9), 3704–3709.
- (20) Bonifas, A. P.; McCreery, R. L. *Nat. Nanotechnol.* **2010**, *5* (8), 612–617.
- (21) Love, J. C.; Estroff, L. A.; Kriebel, J. K.; Nuzzo, R. G.; Whitesides, G. M. *Chem. Rev.* **2005**, *105* (4), 1103–1169.
- (22) Akkerman, H. B.; Blom, P. W. M.; de Leeuw, D. M.; de Boer, B. *Nature* **2006**, *441* (7089), 69–72.
- (23) Akkerman, H. B.; Naber, R. C. G.; Jongbloed, B.; van Hal, P. A.; Blom, P. W. M.; de Leeuw, D. M.; de Boer, B. *Proc. Natl. Acad. Sci. U.S.A.* **2007**, *104* (27), 11161–11166.
- (24) Wang, W. Y.; Lee, T.; Reed, M. A. *Phys. Rev. B* **2003**, *68*, 035416.
- (25) Bumm, L. A.; Arnold, J. J.; Dunbar, T. D.; Allara, D. L.; Weiss, P. S. *J. Phys. Chem. B* **1999**, *103* (38), 8122–8127.
- (26) Cui, X. D.; Zarate, X.; Tomfohr, J.; Sankey, O. F.; Primak, A.; Moore, A. L.; Moore, T. A.; Gust, D.; Harris, G.; Lindsay, S. M. *Nanotechnology* **2002**, *13* (1), 5–14.
- (27) Holmlin, R. E.; Haag, R.; Chabiny, M. L.; Ismagilov, R. F.; Cohen, A. E.; Terfort, A.; Rampi, M. A.; Whitesides, G. M. *J. Am. Chem. Soc.* **2001**, *123* (21), 5075–5085.
- (28) Cui, X. D.; Primak, A.; Zarate, X.; Tomfohr, J.; Sankey, O. F.; Moore, A. L.; Moore, T. A.; Gust, D.; Harris, G.; Lindsay, S. M. *Science* **2001**, *294* (5542), 571–574.
- (29) Beebe, J. M.; Engelkes, V. B.; Miller, L. L.; Frisbie, C. D. *J. Am. Chem. Soc.* **2002**, *124* (38), 11268–11269.
- (30) Akkerman, H. B.; de Boer, B. *J. Phys.: Condens. Matter* **2008**, *20* (1), 20.
- (31) Slowinski, K.; Chamberlain, R. V.; Miller, C. J.; Majda, M. *J. Am. Chem. Soc.* **1997**, *119* (49), 11910–11919.
- (32) Wold, D. J.; Haag, R.; Rampi, M. A.; Frisbie, C. D. *J. Phys. Chem. B* **2002**, *106* (11), 2813–2816.
- (33) Wold, D. J.; Frisbie, C. D. *J. Am. Chem. Soc.* **2001**, *123* (23), 5549–5556.

- (34) Neshet, G.; Shpaisman, H.; Cahen, D. *J. Am. Chem. Soc.* **2007**, *129* (4), 734–735.
- (35) Klauk, H.; Zschieschang, U.; Pflaum, J.; Halik, M. *Nature* **2007**, *445* (7129), 745–748.
- (36) Boulas, C.; Davidovits, J. V.; Rondelez, F.; Vuillaume, D. *Phys. Rev. Lett.* **1996**, *76* (25), 4797–4800.
- (37) Brinkman, W. F.; Dynes, R. C.; Rowell, J. M. *J. Appl. Phys.* **1970**, *41* (5), 1915–1921.
- (38) Beebe, J. M.; Kim, B.; Gadzuk, J. W.; Frisbie, C. D.; Kushmerick, J. G. *Phys. Rev. Lett.* **2006**, *97* (2), 026801.
- (39) Simmons, J. G. *J. Appl. Phys.* **1963**, *34* (1), 238–239.
- (40) Vilan, A. *J. Phys. Chem. C* **2007**, *111* (11), 4431–4444.
- (41) Zang, J.; Huang, M. H.; Liu, F. *Phys. Rev. Lett.* **2007**, *98* (14), 146102.
- (42) Deneke, C.; Songmuang, R.; Jin-Phillipp, N. Y.; Schmidt, O. G. *J. Phys. D: Appl. Phys.* **2009**, *42* (10), 103001.
- (43) Deneke, C.; Sigle, W.; Eigenthaler, U.; van Aken, P. A.; Schutz, G.; Schmidt, O. G. *Appl. Phys. Lett.* **2007**, *90* (26), 263107.
- (44) Gadzuk, J. W.; Plummer, E. W. *Rev. Mod. Phys.* **1973**, *45* (3), 487–548.
- (45) Sze, S. M. *Physics of Semiconductor Devices*; Wiley: New York, 1981.
- (46) Aswal, D. K.; Lenfant, S.; Guerin, D.; Yakhmi, J. V.; Vuillaume, D. *Small* **2005**, *1* (7), 725–729.
- (47) Schroder, D. K. *Semiconductor Materials and Device Characterization*; Wiley: New York, 1998.
- (48) Muller, C.; Khatri, M. S.; Deneke, C.; Fahler, S.; Mei, Y. F.; Urena, E. B.; Schmidt, O. G. *Appl. Phys. Lett.* **2009**, *94* (10), 102510.
- (49) Deneke, C.; Schumann, J.; Engelhard, R.; Thomas, J.; Muller, C.; Khatri, M. S.; Malachias, A.; Weisser, M.; Metzger, T. H.; Schmidt, O. G. *Nanotechnology* **2009**, *20* (4), 045703.
- (50) Huang, G. S.; Mei, Y. F.; Cavallo, F.; Baunack, S.; Coric, E.; Gemming, T.; Bertram, F.; Christen, J.; Fu, R. K. Y.; Chu, P. K.; Schmidt, O. G. *J. Appl. Phys.* **2009**, *105* (1), 016103.

# Hybrid organic/inorganic molecular heterojunctions based on strained nanomembranes

*Carlos Cesar Bof Bufon<sup>1\*</sup>, Juan Diego Ariaz Espinoza<sup>1</sup>, Dominic J. Thurmer<sup>1</sup>, Martin Bauer<sup>1</sup>,  
Christoph Deneke<sup>1§</sup>, Ute Zschieschang<sup>3</sup>, Hagen Klauk<sup>3</sup>, Oliver G. Schmidt<sup>1,2</sup>*

<sup>1</sup> Institute for Integrative Nanosciences, IFW-Dresden, Helmholtz Str. 20, 01069 Dresden, Germany

<sup>2</sup> Material Systems for Nanoelectronics, TU-Chemnitz, Reichenhainer Str 70, 09107 Chemnitz,  
Germany

<sup>3</sup> Max Planck Institute for Solid State Research, Heisenberg Str. 1, 70569 Stuttgart, Germany

\*c.bufon@ifw-dresden.de

## SUPPORTING INFORMATION

### **1. Au-alkanethiol SAM/Au heterojunctions**

#### *a. Fabrication of the Au-alkanethiol SAM/Au heterojunctions*

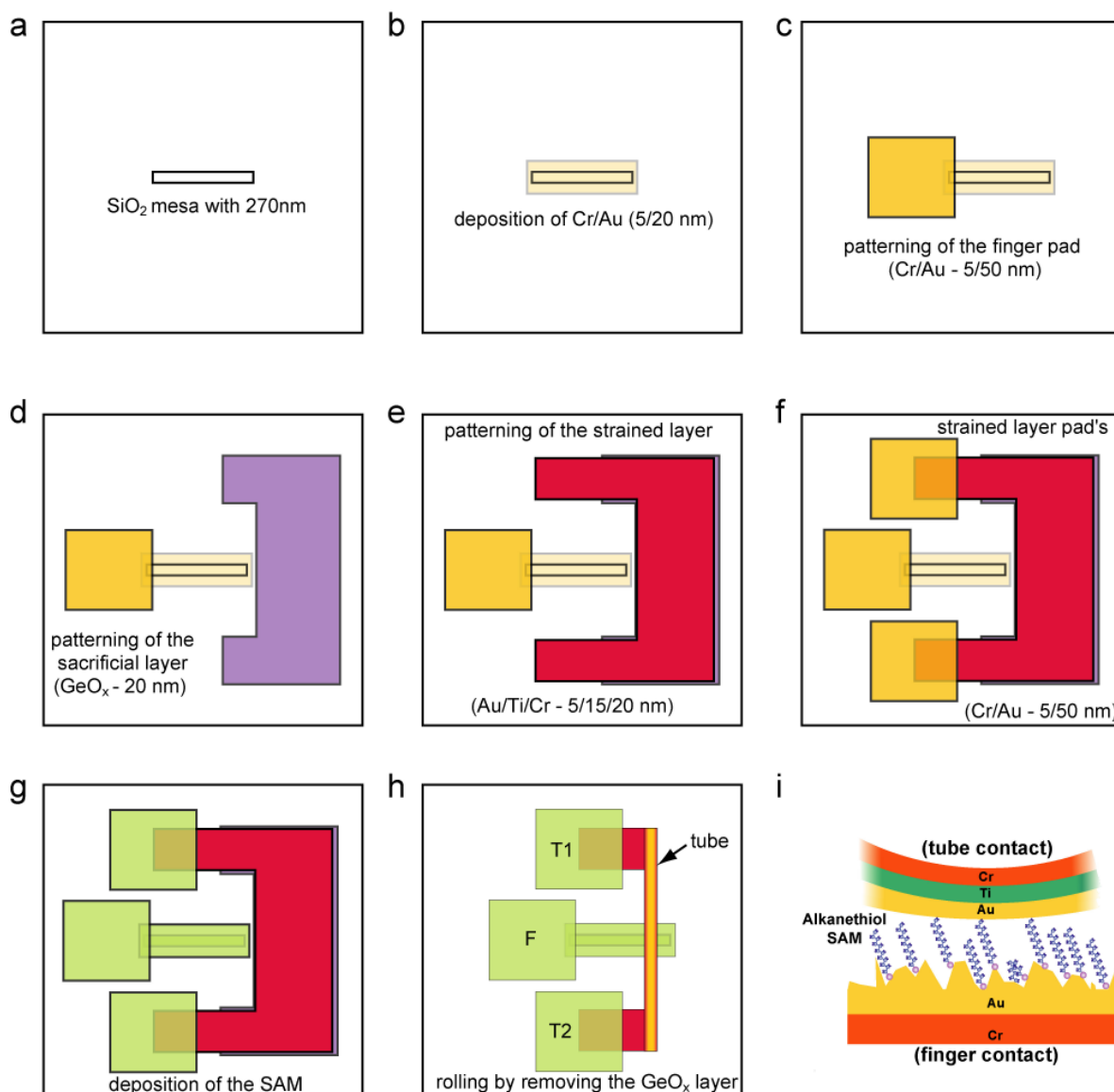
The Au-alkanethiol SAM/Au heterojunctions were fabricated on Si (100) wafers covered by 1  $\mu\text{m}$  SiO<sub>2</sub>. The first step is the creation of the finger structure by patterning and etching 270 nm of the SiO<sub>2</sub> layer in 10% HF for a few seconds (Supplementary figure 1a). Afterwards the mesa is covered by a Cr/Au (5/20 nm) conducting layer (Supplementary figure 1b) by thermal evaporation, where the roughness of the metal film covering the finger was kept below the SAM chain length (i.e.  $\sim 0.36$  nm RMS). This low roughness was of importance, since devices with high roughness gold films displayed

short circuit behaviour. In all steps, the patterning is done by conventional photolithography. Next in the sequence, as illustrated in Supplementary figure 1c, a contact pad is patterned overlapping the finger structure by depositing Cr/Au (5/50 nm) again. Before depositing the strained layer, a GeO<sub>x</sub> layer (20 nm) is patterned as illustrated in Supplementary figure 1d. The fabrication process used for preparing the sacrificial layer is described in detail elsewhere<sup>1</sup>. Next, the strained layer, consisting of a tri-metallic nanomembrane Au/Ti/Cr (5/15/20 nm), is deposited by electron-beam evaporation on top of the GeO<sub>x</sub> sacrificial layer (Supplementary figure 1e). Here, the Ti/Cr bimetallic layer creates the strain gradient necessary for tube formation, while the bottom Au layer is used as the contact layer for the SAM after rolling. Lastly, the pads for the strained layer (later the tube structure) are fabricated (Supplementary figure 1f).

Preceding the rolling process, alkanethiol self-assembled monolayers (SAM), with chain lengths ranging from 8 to 16 carbon atoms, are grown on top of the gold finger (Supplementary figure 1g). To grow the SAM, we immerse the device structures into a freshly prepared ~5 mM alkanethiol in methanol<sup>2</sup> solution for 24 hours in an argon-filled glove box. After SAM growth, the sample is rinsed in clean methanol and dried with a N<sub>2</sub> flow.

Next, the rolling is performed, facilitated by the self-release of the strained metallic nanomembrane through selective removal of the GeO<sub>x</sub> sacrificial layer in pure deionised H<sub>2</sub>O (Supplementary figure 1h). The contact between the tube and finger is formed after 2 hours of rolling. Alternatively, the required rolling time can also be controlled by changing the GeO<sub>x</sub> composition and etching solution<sup>1</sup>.

After the rolling process, the tube-like electrode rests on top of the metallic finger establishing an electrical connection through the SAM (Supplementary figure 1h). Notice that the contact to the tube electrode is established by the Au layer which is the outermost layer of the tube (Supplementary figure 1i). Finally, after completion the samples are transferred from H<sub>2</sub>O to methanol and subsequently dried in a vacuum chamber for 24 hrs.



**Supplementary Figure 1:** (a-h) Fabrication scheme of the Au-alkanethiol SAM/Au heterojunction. (i), Au-alkanethiol SAM/Au interfaces (not to scale).

*b. Contact angle measurements*

In order to evaluate the quality of the alkanethiol layers prepared on the Au surface as well as the changes of such layer after long time in the rolling solution (H<sub>2</sub>O), we performed contact angle measurements in control-samples using the water droplet method. The control samples were prepared by depositing a Cr/Au (5/20 nm) thin film on top of the Si/SiO<sub>2</sub> substrate. This deposition on the control samples was carried out simultaneously with the coating of the finger structure for the measured devices (Supplementary figure 1b). Consequently, the roughness of both finger and control samples are

identical. Similarly, the growth of the alkanethiol SAM was performed simultaneously on the finger structure and on the control samples. After the SAM growth and before the rolling procedure the contact angle measurements revealed angles larger than  $103^\circ$ , regardless of the SAM chain length (see the column “before rolling ” in the Supplementary Table 1). This indicates a hydrophobic Au surface covered by a well-ordered SAM. To check for any possible damage to the SAM due to the long time exposure in the rolling solution, the control samples were left in H<sub>2</sub>O for more than 12 hours (much longer than the rolling time) before measuring once more the contact angle. As shown in Supplementary Table 1, the SAMs do not suffer significant damage from the long immersion in the rolling solution.

<i>Alkanethiol</i>	<i>Before rolling (<math>\theta_s</math>)</i>	<i>After rolling (<math>\theta_s</math>)</i>
Octanethiol (C8)	105	103
Decanethiol (C10)	106	104
Dodecanethiol (C12)	109	106
Tetradecanethiol (C14)	114	115
Hexadecanethiol (C16)	115	110

**Supplementary Table 1:** Contact angle of alkanethiol modified Au surfaces determined immediately after the SAM deposition (before rolling) and after leaving the samples immersed in water for more than 12 hours (much longer than the rolling time).

*c. Contact resistance in the Au-alkanethiol SAM/Au heterojunction*

In order to measure the Au-alkanethiol SAM/Au heterojunction, a voltage bias was applied between the finger’s pad (F in supplementary figure 1h) and the tube’s pad (T1 or T2 in supplementary figure 1h). By measuring the resistance of several junctions rolled without molecules (i.e Au-finger/Au-tube between F and T1 for instance), we were able to determine the devices series resistance ( $5 \pm 1 \Omega$ ). In addition, the electrical resistance of the tube was measured between T1 and T2 and was found to be as small as  $3 \pm 1 \Omega$ .

In Fig. 1, by extrapolating the junction differential resistance to zero  $\text{CH}_2$  units<sup>3</sup>, the total contact resistance  $R_0$  ( $\sim 8.9 \Omega$ ) was also determined from the data fit. By subtracting the series resistance due to the finger and tube structures ( $5 \pm 1 \Omega$ ) from  $R_0$ , we determined the effective contact resistance of the Au-alkanethiol SAM/Au heterojunction as  $3.9 \pm 1 \Omega$ . For a contact area of  $\sim 15 \text{ nm}^2$ , which is often assumed when using conducting probe atomic microscopy<sup>3,4</sup> to contact molecular layers, the effective contact resistance obtained from  $R_0$  extrapolates to  $70 \pm 18 \text{ k}\Omega$  taking into account the contact area of  $\sim 0.27 \mu\text{m}^2$ . This extrapolated value agrees with the values previously reported for identical alkanethiols monolayers<sup>3</sup>.

## **2. Molecular beam epitaxy of the semiconductor stacking layer.**

The semiconductor samples used in this work were fabricated by solid source molecular beam epitaxy (MBE). All layer structures were grown on deoxidized epi-ready GaAs (001) wafers with an intrinsic n-doping of  $(1-5) \times 10^{18}$ . Beryllium was used for p-doping while n-doping was achieved using silicon. Target doping concentrations were  $2 \times 10^{19}$  and  $5 \times 10^{18}$  for p- and n-, respectively. Typical growth rates were below 0.8 ML/second for all III-V materials. The growth temperature was kept at 70 °C below the transition temperature between (2x4) and the c(4x4) reconstruction. Crystalline quality was checked continuously during the entire growth process using RHEED.

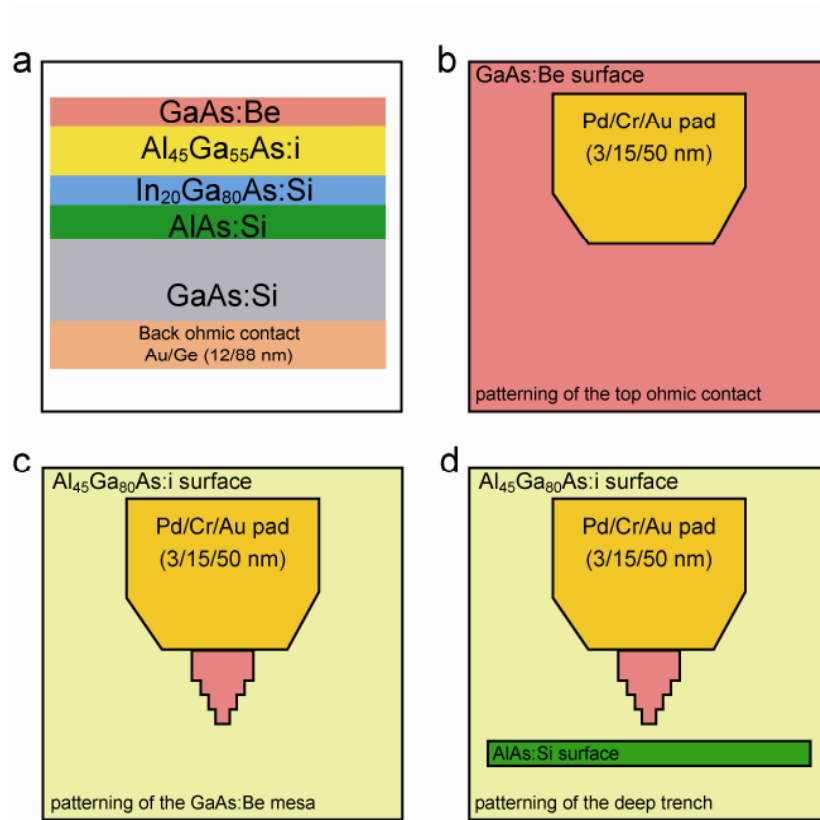
## **3. Fabrication of the p:GaAs-C16PA/n:InGaAs and p:GaAs/n:InGaAs heterojunctions**

### *a. Common steps for both junctions*

The back electrical contact was created by thermal evaporation of 12 nm Ge and 88 nm Au on the back side of the heavily n-doped GaAs wafer (Supplementary figure 2a). Afterwards the sample was annealed at 430°C for 1 minute to diffuse the Ge into the sample and create an ohmic contact.

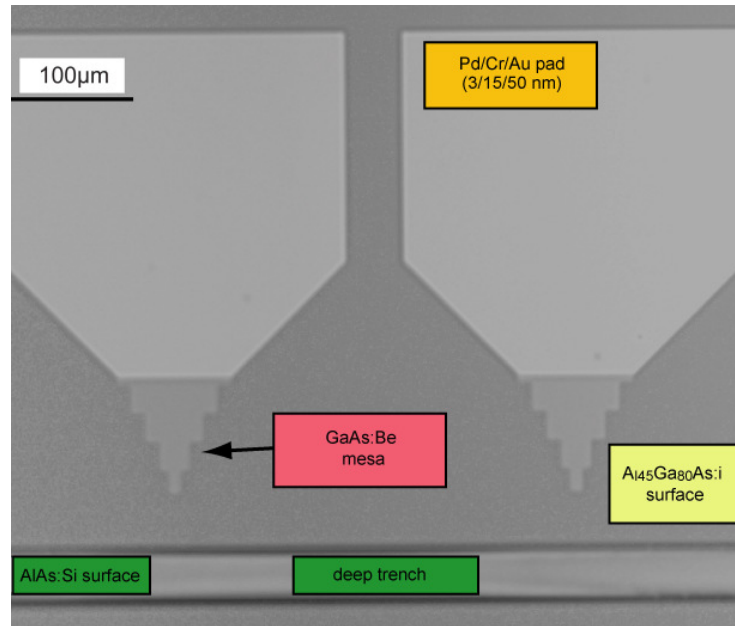
To contact the p-doped GaAs layer on the top-side of the sample a shallow ohmic contact with 3 nm Pd, 15 nm Cr and 50 nm Au was deposited by e-beam evaporation using photolithography and metal lift-off (Supplementary figure 2b). Next, a mesa structure was patterned by photolithography, defining the active area (p:GaAs mesa) by etching away  $\sim 25 \text{ nm}$  of the top p:GaAs/AlGaAs layers in a solution of

phosphoric acid/hydrogen peroxide/water (1:10:500) on the rest of the sample (Supplementary figure 2c).



**Supplementary Figure 2:** (a) Semiconductor layer structure grown by MBE including the back Ohmic contact. (b-d) fabrication steps for the preparing the hybrid p:GaAs-C16PA/n:InGaAs and p:GaAs/n:InGaAs heterojunctions.

Prior to the SAM deposition, a deep trench is etched down to the n:AlAs sacrificial layer using a solution of  $\text{K}_2\text{Cr}_2\text{O}_7/\text{HBr}/\text{CH}_3\text{COOH}$  (Supplementary figure 2d). Afterwards the structure is ready for rolling by underetching the n:AlAs sacrificial layer. Supplementary figure 3 shows a SEM image of the device before rolling.



**Supplementary Figure 3:** Top view of the planar semiconducting structure before rolling up.

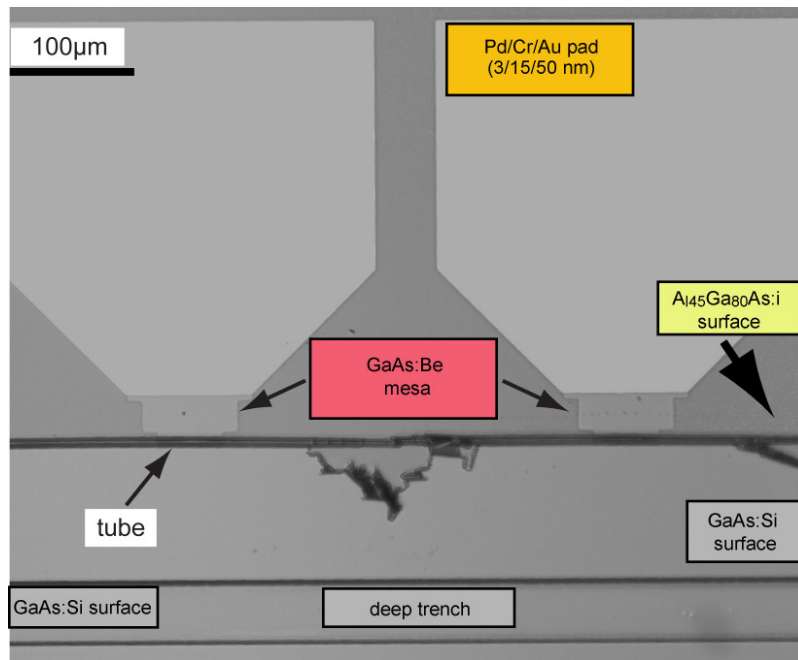
*b. Formation of the p:GaAs-C16PA/n:InGaAs heterojunction*

For preparing the p:GaAs-C16PA/n:InGaAs, the processed substrate was first dipped in a 5% HCl:H<sub>2</sub>O solution for 15 s to remove the native oxide from the p:GaAs surface layer. Immediately after the oxide removal, the sample was immersed in a solution of 5 mM hexadecylphosphonic acid (C16PA) in ethanol for 24 hours to deposit the SAM. The SAM deposition was completed in an argon-filled glove box. After the SAM growth the sample was rinsed in pure ethanol and dried in N<sub>2</sub>.

With the SAM deposited, the next step to form the p:GaAs-C16PA/n:InGaAs heterojunction was rolling the nanomembrane in a solution of HF/H<sub>2</sub>O (3.1 vol%) for 30 s. The contact angle measurements indicate that no damage to the C16PA layer on the p:GaAs is created by immersing the sample in the rolling solution for at least 3 minutes. Before and after rolling, the measured contact angle for the C16PA on p:GaAs was 109° and 108°, respectively. In order to stop the rolling, the sample was transferred to water and then ethanol. Afterwards, the rolled-up sample was left in mechanical vacuum for 12 hours prior to the measurements.

*c. Formation of the p:GaAs/n:InGaAs heterojunction*

Prior to rolling, the processed substrates were dipped in a solution of 5% of HCl in water for 15 s to remove the native oxide from the p:GaAs surface layer. Next, rolling was performed by immersing the structure in a solution of HF/H<sub>2</sub>O (3.1 vol%) for 30 s. This time is enough for the released nanomembrane to perform ~1.5 rotation. The number of windings can be controlled by the rolling time. For instance, in Supplementary Figure 4, an image of a rolled device comprising ~3 windings is shown. In this device the tube electrode has a diameter of about 10 μm.



**Supplementary Figure 4:** Top view of the device structure after rolling up. The rolling occurs by the selective removal of the n:AlAs sacrificial layer in low concentration HF solution.

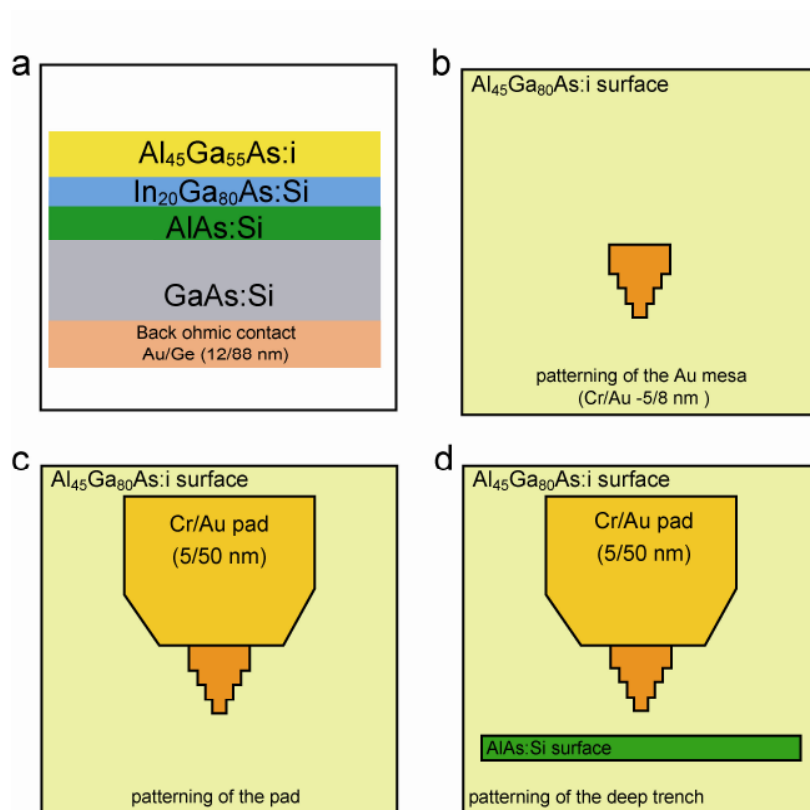
#### **4. Fabrication of the Au-C16S/n:InGaAs and Au/n:InGaAs heterojunctions**

*a. Common steps for both junctions*

Similar to the p:GaAs-C16PA/n:InGaAs heterojunction, the back electrical contact is realised by thermal evaporation of 12 nm Ge and 88 nm Au on the back side of the heavily n-doped GaAs wafer (Supplementary Figure 5a which is annealed at 430 °C for 1 min afterwards).

For this device concept, the Au top electrode was fabricated by depositing 5 nm Cr followed by 8 nm Au (Supplementary Figure 5b) to create a mesa structure. The contact pad slightly overlaps the Au

electrode (Supplementary Figure 5c) and was made by the electron-beam deposition of Cr/Au (5/50 nm). Furthermore, the AlGaAs:i layer was etched ~40 nm below the Cr/Au mesa by using a solution of phosphoric acid/hydrogen peroxide/water (1:10:500). This procedure was used to improve the rolling dynamics of the semiconducting nanomembrane. The last step consists of a deep trench which is opened to allow the underetching of the AlAs:Si sacrificial layer (Supplementary Figure 5d) which was done by immersing the sample in  $K_2Cr_2O_7/HBr/CH_3COOH$  solution for a few seconds.



**Supplementary Figure 5:** (a) Semiconductor layer structure grown by MBE including the back Ohmic contact. (b-d), fabrication steps for the preparing the hybrid Au-C16S/n:InGaAs and Au/n:InGaAs heterojunctions.

*b. Formation of the Au-C16S/n:InGaAs heterojunction*

Prior to rolling the samples were immersed in a freshly prepared solution of ~5mM hexadecanethiol (C16S) in ethanol for 24 hours. The growth was performed in an Argon glove box. After the SAM growth, the samples were rinsed in pure ethanol to remove physisorbed molecules.

The rolling process takes place by immersing the sample in a solution of HF/H<sub>2</sub>O (3.1 vol%) for 30s. Similar to the C16PA grown on p:GaAs, the C16S on Au did not exhibit a clear sign of damage after immersed in the rolling solution. Before and after rolling the measured contact angle was 105° and 106°, respectively. To stop the rolling, the samples were transferred to water and then to pure ethanol. Afterwards, the rolled sample was left in mechanical vacuum for 12 hours previously the measurements.

*c. Formation of the Au/n:InGaAs heterojunction*

In order to prepare the Au/n:InGaAs the sample is rolled without the SAM deposition step after the opening of the deep trench in a solution of HF/H<sub>2</sub>O (3.1 vol%) for 30s.

**5. Roughness of the semiconducting interfaces**

In this section we discuss the smoothness of the interfaces in the rolled-up structures. In fact, the interfaces have been carefully studied by us for several material systems<sup>5</sup>. Basically, for the **Au-C16S/n:InGaAs** heterojunctions two interfaces are of interest: the top interface of the Au layer and the newly formed interface by removing the AIAs sacrificial of the bottom n:InGaAs. For the the p:GaAs-C16PA/n:InGaAs heterojunction, the top interface of interest is the p:GaAs. The internal interface of a rolled-up semiconductor/organic layer system is studied in detail elsewhere<sup>6</sup>. From our previous studies, we show that the rolled-up layers inherit the roughness of the epitaxial layer which is some monolayer fluctuations. HR-TEM images<sup>7</sup> obtained for similar structures depict the high quality of the interface. Additionally, these images reveal an atomic smooth surface of the bottom as well as the top semiconductor layers.

As mentioned above, the releasing of the semiconducting nanomembrane takes place in a solution of HF/H<sub>2</sub>O (3.1 vol%) for 30s. That the HF used to remove the AIAs does not attack and therefore roughen the GaAs interface is not only demonstrated by the extreme high selectivity<sup>8</sup>, but also by our ability to release membranes as thin as 5 monolayers<sup>6</sup>: If any roughing were to take place, such thin membranes could not be released.

## 6. Characterization

### a. Characterization techniques

The as-processed devices were imaged using a Zeiss Cross-beam® with 5-20 kV acceleration voltage.

All *i-v* characteristics were measured using a Keithley 2635A source-meter. The low-temperature measurements were performed in a Lakeshore helium flow probe-station cryostat.

### b. Heterojunctions based on semiconducting tubes: yield

Each sample (with and without SAM) consists of arrays of junctions varying between 10 and 210 devices, depending on the mask design and pads size, with a yield ranging from 85% to 90%. The breaking of the tubes during the rolling procedure is the main reason for the yield losses. If we consider only the perfect rolled tubes, the yield of working junctions increases to 95% to 100%. In this case, the main factors responsible for the yield losses are the defects on the semiconductor stacking layer and the small damages occurred during the photolithographic process. In order to evaluate the yield, all devices on a chip were characterized by *i-v* measurements at room temperature. On the same chip all *i-v* characteristics agree qualitatively. For the Au-C16S/n:InGaAs heterojunction a variation of the current magnitude is of ~ 9% from device to device. The p:GaAs-C16PA/n:InGaAs heterojunctions show a better statistics with a current variation of maximum 5% for devices on the same chip. At least 7 devices for each type of heterojunction were fully characterized at low temperature.

## 7. References

---

<sup>1</sup> Bufon, C. C. B.; Gonzalez, J. D. C.; Thurmer, D. J.; Grimm, D.; Bauer, M.; Schmidt, O. G. *Nano Letters* 2010, 10, (7), 2506-2510.

<sup>2</sup> Porter, M. D.; Bright, T. B.; Allara, D. L.; Chidsey, C. E. D. *Journal of the American Chemical Society* 1987, 109, (12), 3559-3568.

<sup>3</sup> Beebe, J. M.; Engelkes, V. B.; Miller, L. L.; Frisbie, C. D. *Journal of the American Chemical Society* 2002, 124, (38), 11268-11269.

---

<sup>4</sup> Wold, D. J.; Frisbie, C. D. *Journal of the American Chemical Society* 2001, 123, (23), 5549-5556.

<sup>5</sup> Deneke, C.; Songmuang, R.; Jin-Phillipp, N. Y.; Schmidt, O. G. *Journal of Physics D-Applied Physics* 2009, 42, (10), 103001.

<sup>6</sup> Deneke, C.; Zschieschang, U.; Klauk, H.; Schmidt, O. G. *Applied Physics Letters* 2006, 89, (26), 263110.

<sup>7</sup> Deneke, C.; Schumann, J.; Engelhard, R.; Thomas, J.; Sigle, W.; Zschieschang, U.; Klauk, H.; Chuvilin A.; O. G. Schmidt, *Phys. Status Solidi C* 2008, 5, 2704.

<sup>8</sup> Wu, X. S.; Coldren, L. A.; Merz, J. L. *Electron. Lett.* 1985, 21, 558.